



An alternative reaction for heme degradation catalyzed by the *Escherichia coli* O157:H7 ChuS protein: Release of hematinic acid, tripyrrole and Fe(III)



Yannick H. Ouellet^a, Cheikh Tidiane Ndiaye^a, Stéphane M. Gagné^a, Anne Sebilo^a, Michael D.L. Suits^{b,1},
Éric Jubinville^a, Zongchao Jia^b, Anabella Ivancich^{c,*}, Manon Couture^{a,*}

^a Département de Biochimie, de Microbiologie et de Bio-informatique, IBIS and PROTEO, Université Laval, Québec G1V 0A6, Canada

^b Department of Biomedical and Molecular Sciences, Queen's University, Kingston, Ontario K7L 3N6, Canada

^c CNRS, Unité de Recherche Mixte CNRS/Aix-Marseille Université (UMR 7281), Laboratoire de Bioénergétique et Ingénierie des Protéines, 13009 Marseille, France

ARTICLE INFO

Article history:

Received 7 July 2015

Received in revised form 8 October 2015

Accepted 1 November 2015

Available online 10 November 2015

Keywords:

Heme degradation

Verdoheme

Iron

ChuS

EPR spectroscopy

Hematinic acid

ABSTRACT

As part of the machinery to acquire, internalize and utilize heme as a source of iron from the host, some bacteria possess a canonical heme oxygenase, where heme plays the dual role of substrate and cofactor, the later catalyzing the cleavage of the heme moiety using O₂ and electrons, and resulting in biliverdin, carbon monoxide and ferrous non-heme iron. We have previously reported that the *Escherichia coli* O157:H7 ChuS protein, which is not homologous to heme oxygenases, can bind and degrade heme in a reaction that releases carbon monoxide. Here, we have pursued a detailed characterization of such heme degradation reaction using stopped-flow UV-visible absorption spectrometry, the characterization of the intermediate species formed in such reaction by EPR spectroscopy and the identification of reaction products by NMR spectroscopy and Mass spectrometry. We show that hydrogen peroxide (in molar equivalent) is the key player in the degradation reaction, at variance to canonical heme oxygenases. While the initial intermediates of the reaction of ChuS with hydrogen peroxide (a ferrous keto π neutral radical and ferric verdoheme, both identified by EPR spectroscopy) are in common with heme oxygenases, a further and unprecedented reaction step, involving the cleavage of the porphyrin ring at adjacent meso-carbons, results in the release of hematinic acid (a monopyrrole moiety identified by NMR spectroscopy), a tripyrrole product (identified by Mass spectrometry) and non-heme iron in the ferric oxidation state (identified by EPR spectroscopy). Overall, the unprecedented reaction of *E. coli* O157:H7 ChuS provides evidence for a novel heme degradation activity in a Gram-negative bacterium.

© 2015 Elsevier Inc. All rights reserved.

1. Introduction

Iron acquisition is vital for pathogens survival within the host [1,2]. Since the most abundant source of iron is the heme of hemoglobin and of other heme binding proteins of the host, bacteria have developed an impressive machinery to acquire, internalize and utilize heme as a source of iron (see [3] for review). Infections by *Escherichia coli* O157:H7 can cause severe gastroenteritis in humans, which sometimes evolve to the life-threatening hemolytic uremic syndrome condition [4,

5]. Bacterial growth of *E. coli* O157:H7 isolated from infected patients is stimulated in the presence of heme and hemoglobin, suggesting that heme may be an important signaling molecule for the up-regulation of factors contributing to host colonization and virulence [6]. This bacterium may also induce hemolytic lesions to gain access to the host nutrients [6]. In this context, it is interesting that the analysis of the *E. coli* O157:H7 genome revealed that this bacterium contains a gene cluster, *chuASTUVWXY*, highly similar to the *shu* gene cluster of *Shigella* involved in heme internalization and processing pathway [7].

In Gram-negative bacteria that possess a gene cluster for heme internalization, heme either free in solution, bound to proteins such as hemoglobin or captured via specialized protein chelators, is first anchored onto the pathogen surface via an outer membrane TonB-dependent receptors that also actively transport the heme across the outer membrane [3]. An ABC (ATP binding cassette) permease that transport heme across the inner membrane finalizes the heme internalization process [3]. In *E. coli* O157:H7, these functions are assigned to the outer membrane heme receptors ChuA and Hma [8,9] and to the permease composed of three proteins; the periplasmic binding protein (ChuT), the integral membrane protein (ChuU) and the ATPase

Abbreviations: ChuS, ChuS protein containing a N-terminal 6-histidine tag; apo-ChuS, heme-free ChuS; holo-ChuS, heme-bound ChuS; HO, heme oxygenase; HO-1, heme oxygenase-1; ABC, ATP binding cassette; HRP, horseradish peroxidase; ms, millisecond; ADHP, 10-acetyl-3,7-dihydroxyphenoxazine; ABTS, 2,2'-azino-bis(3-ethylbenzothiazoline-6-sulfonic acid); TFA, trifluoroacetic acid; EPR, electron paramagnetic resonance; NMR, nuclear magnetic resonance; HS, high-spin; LS, low-spin; PDA, photodiode array; PMT, photomultiplier tube; sh, shoulder; MS, mass spectrometry.

* Corresponding authors.

E-mail addresses: aivancich@imm.cnrs.fr (A. Ivancich), Manon.Couture@bcm.ulaval.ca (M. Couture).

¹ Present address: Department of Chemistry, Wilfrid Laurier University, Waterloo, Ontario N2L 3C5, Canada.

(ChuV) [10]. Once inside the cytoplasm, the heme may be bound by chaperones and transferred to other proteins or it may be metabolized to release the sequestered iron. This later reaction may be carried out by a heme oxygenase (HO) in Gram-negative bacteria that possess the gene encoding this enzyme. Like the HO from higher organisms, bacterial HO uses heme both as a substrate and as a cofactor to catalyze the opening of the porphyrin ring thus producing biliverdin and carbon monoxide and liberating the iron [11–15].

The reaction carried out by HO occurs at the heme-bound active site and requires electrons, which are provided by cytochrome P450 reductase/NADPH or ascorbate *in vitro*, and molecular oxygen [12,13,16,17]. The complete reaction cycle requires 7 electrons in total and generates carbon monoxide, ferrous iron and biliverdin. The mechanism of the HO reaction has been elucidated and the detailed picture of the reactive intermediates of the catalytic reaction emerged from biochemical studies in heme oxygenase 1 (HO-1) and a bacterial HO (HmuO), using various spectroscopy techniques (reviewed in [11–14,16]). In the HO reaction, after the heme is first reduced and binds oxygen, the heme-bound oxygen is activated by a second electron and a proton to form a hydroperoxy complex ($\text{Fe}^{\text{III}}\text{-OOH}$) from which hydroxylation of the heme occurs and meso-hydroxyheme is formed. The initial oxygenated complex of HO was characterized by resonance Raman spectroscopy [18,19] and X-ray crystallography [19] which revealed an unusually highly-bent geometry of the heme-bound O_2 . The short-lived hydroperoxy complex was formed by cryoreduction from the oxidized enzyme and was characterized by EPR and ENDOR spectroscopies [20]. Notably, this intermediate was shown to be competent to hydroxylate the heme to produce meso-hydroxyheme [20]. The details about the coordination and electronic structure of the meso-hydroxyheme intermediate, which is stable in absence of molecular oxygen and could exist in three equilibrium forms, was probed by EPR and resonance Raman spectroscopies [21,22]. The subsequent intermediate, verdoheme, which is formed spontaneously by the reaction of meso-hydroxyheme with molecular oxygen, was probed with NMR [23] and resonance Raman spectroscopies [21] and shown to be in a 6-coordinate state. The complex of verdoheme with HO-1 was also characterized by X-ray crystallography to get a better picture of the mechanism for the opening of the porphyrin ring to the final product biliverdin [24,25]. The enzymatic degradation of heme by mammalian HOs occurs quite selectively at the alpha-meso-carbon. On the contrary, the chemical oxidation of heme in the presence of excess reductant and molecular oxygen, termed coupled oxidation, is rather unspecific attacking essentially all four meso-carbons [26,27].

Bacterial HOs similar to those of mammalian, termed canonical HOs, are found in several pathogens including *Corynebacterium diphtheria* [19,28,29], *Neisseria meningitidis* [30,31] and *Pseudomonas aeruginosa* [32]. In Gram-positive bacteria, the LsdG family of proteins performs a similar function to HOs although they are not structurally related and yield porphyrin products different from biliverdin [33–35]. Notably, a HO is apparently absent in *E. coli* strains, including O157:H7, based on genomic data mining. Thus, the fate of the heme once it reaches the cytoplasm is not clearly understood in *E. coli* O157:H7 or in bacteria that have no homologs of canonical HOs or LsdG [3].

We previously reported that the ChuS protein of *E. coli* O157:H7, a protein encoded by the *chuS* gene of the *chu* gene cluster, is able to bind and degrade heme in a reaction that releases carbon monoxide [36]. The physiological role for the ChuS protein in iron acquisition remains however to be established [3]. Since this protein has no structural homology to canonical HOs neither to the LsdG family of proteins [36, 37], we have pursued a thorough investigation of its heme degradation mechanism. In this work, we present a detailed analysis of the heme degradation reaction by ChuS using stopped-flow optical absorption spectroscopy and EPR spectroscopy and we identified reaction products by NMR spectroscopy and mass spectrometry (MS) in order to gain further knowledge about the role of proteins of the heme acquisition pathway of *E. coli* O157:H7 and of other bacteria. We show that the heme

within ChuS reacts with H_2O_2 in the low micromolar range and we provide evidence on ferric (not ferrous) iron being released upon cleavage of the heme by a mechanism that differs from that of the canonical HOs.

2. Material and methods

2.1. Chemicals and reagents

Hemin, catalase, sodium ascorbate, ABTS, guaiacol and horseradish peroxidase (HRP) were from Sigma. Biliverdin-hydrochloride was from Frontier Scientific (Newark, DE).

2.2. ChuS expression and purification

The expression and purification of the recombinant apo-ChuS, with a N-terminal tag composed of 6 histidine residues, was performed in accordance with our previously published method [36]. As a control to verify that the histidine tag was not involved in the heme degradation activity of ChuS, we also expressed and purified the ChuS protein without any tag (Supp. material). The histidine-tagged and untagged proteins degraded heme similarly using ascorbate (Fig. 1 and Supp. Fig. 1). All measurements reported in this study were obtained with the histidine-tagged protein for which the crystal structure is known [36,37]. Protein purity was verified by SDS-PAGE. As purified, the ChuS protein is devoid of heme but displays a light purple color presumably because the enzyme is active inside the bacteria and a fraction of the protein contains a porphyrin degradation product [36]. This product can be extracted using butanol as a solvent (see Section 2.8). Protein concentration was quantified by the Bradford method.

2.3. Preparation of heme-bound ChuS (Holo-ChuS)

Holo-ChuS was prepared by adding a six-fold molar excess of hemin (solubilized in 15 mM NaOH and neutralized in 50 mM Tris-HCl pH 8) to the apo-protein solution and incubated 15–30 min at room temperature. Removal of excess heme was performed by loading the heme-protein mixture onto a 10 ml DEAE Sepharose Fast Flow column (GE Healthcare) equilibrated with 50 mM Tris-HCl pH 8. After washing with the same buffer, the holo-protein complexes was eluted with 50 mM Tris-HCl pH 8 buffer containing 250 mM NaCl. The collected fractions were dialyzed (Spectrapor membranes, 10 kDa MWCO) against 0.1 M sodium phosphate pH 7 overnight at 4 °C. The dialysate was concentrated using a 10 kDa cut-off Centricon (Millipore) and kept at –80 °C. The protein and heme contents were quantified by the Bradford (Bio-Rad Laboratories) and pyridine heme methods, respectively [38]. We determined that holo-ChuS contains one heme per monomer of protein (1.1 ± 0.1). All protein concentrations throughout this paper are reported based on the heme content. All experiments were performed in 0.1 M sodium phosphate buffer at pH 7.0.

2.4. UV-vis characterization of heme degradation

The characterization of ChuS heme degradation reaction was studied at 20 °C with either sodium ascorbate or with hydrogen peroxide on a Cary 3E spectrophotometer (Varian) equipped with a temperature-controlled multicell holder. Sodium ascorbate was added to a 10 μM solution of holo-ChuS to a final concentration of 100 μM . The absorption spectra of ChuS upon addition of sodium ascorbate were recorded at 5 minute intervals during 60 min. Where indicated, catalase (50 to 300 U) was added to the reaction mixtures. For the peroxide-driven reaction, hydrogen peroxide (final concentrations of 5–20 μM) was added to a 10 μM holo-ChuS. Heme degradation was also followed by acquiring the optical absorption spectra at 5 minute intervals. The concentration of the H_2O_2 stock solution was determined using an absorption coefficient of $43.6 \text{ M}^{-1} \text{ cm}^{-1}$ at 240 nm [39]. To obtain the spectra of the

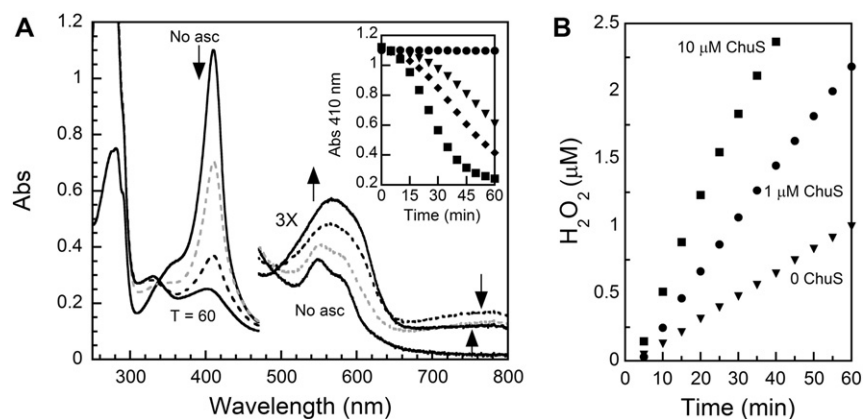


Fig. 1. The degradation of heme by ChuS using ascorbate. **A** – The degradation of heme was initiated by the addition of ascorbic acid (100 μM final concentration) to a solution containing holo-ChuS (10 μM , black line) in sodium phosphate buffer pH 7.0. The optical absorption spectra were recorded over the course of 60 min at 20 $^{\circ}\text{C}$. The spectra recorded at 25 min (gray and dashed line), 40 min (black dashed line) and 60 min (solid black line labeled T = 60) are shown. The inset shows the variation in absorbance at 410 nm plotted as a function of time (squares) and for identical reactions containing 150 U (diamonds) and 300 U (triangles) catalase and with no ascorbic acid added (circles). **B** – The amount of H_2O_2 formed in aerobic solutions containing ascorbate with or without heme-bound ChuS was followed from the increased fluorescence signal at 590 nm (Exc. at 544 nm) caused by the oxidation of ADHP to resorufin by HRP as it used the H_2O_2 formed in solution. The reactions were recorded in 0.1 M sodium phosphate buffer pH 7 and contained either 100 μM sodium ascorbate (triangles), 100 μM sodium ascorbate and 1 μM ChuS (circles) or 100 μM sodium ascorbate and 10 μM ChuS (squares).

pyridine complex, pyridine was added at a final concentration of 16% (v/v) to solutions of ferric ChuS that had reacted with hydrogen peroxide for 100 s or 60 min, the precipitated protein was removed by ultrafiltration (10 kDa cut-off) and the optical spectra were recorded immediately.

2.5. Quantification of hydrogen peroxide

The amount of H_2O_2 formed in an aerobic solution of sodium ascorbate and in the presence of heme-bound ChuS, was quantified using the OxySelect H_2O_2 quantification assay kit (Cell Biolabs Inc.). This system uses HRP and the substrates 10-acetyl-3,7-dihydroxyphenoxazine (ADHP) and hydrogen peroxide to produce fluorescent resorufin. A calibration curve obtained with known amounts of H_2O_2 was used to convert the intensity of the fluorescence signal to actual H_2O_2 concentrations. The fluorescence emission was measured at 590 nm from excitation at 544 nm with a Fluoroskan Ascent FL (Termo LabSystems).

2.6. Stopped-flow UV-vis electronic absorption characterization of heme degradation

We used a stopped-flow spectrometer (Applied Photophysics SX.18MV-R) equipped with a photomultiplier tube (PMT) for the measurement of variations in optical absorbance at single-wavelengths and with a photodiode array (PDA) detector to obtain optical absorption spectra versus time data sets. The dead-time of the stopped-flow was 1.28 ms. In PDA mode, the spectral integration time was 2.56 ms. The 10 mm optical path length of the observation window was used and the monochromator slit widths were adjusted at 1.5 mm. The mixing unit of the stopped-flow was placed inside a glove box, which ensured that good anaerobic conditions were obtained when required (less than 5 ppm O_2 inside the glove box). For anaerobic work, the buffer was equilibrated to the glove box atmosphere for 24 h prior to the experiments. Protein samples and H_2O_2 were flushed with argon for 45 min before being brought into the glove box and used immediately. Data analysis was done using singular-value decomposition with the Specfit software (Spectrum Software Associates) to fit the time-dependent spectra and obtain the observed transition rate constants (k_1, k_2, \dots, k_n) between species. A two-step model ($A \rightarrow B \rightarrow C$) was used, in which A was the ferric holo-ChuS, B was an intermediate state displaying a weak broad band centered in the visible region (named

734 nm species) and C was the species with a broad intense band centered at 565 nm (named 565 nm species).

2.7. Electron paramagnetic resonance spectroscopy

The 9-GHz EPR spectra were recorded on a Bruker EleXsys E500 spectrometer equipped with a standard Bruker ER 4102 X-band resonator and a liquid helium cryostat (Oxford Instruments, ESR 900). A 50 mM sodium phosphate buffer pH 7.0 was used for all EPR experiments on ChuS. The protein concentration was 670 μM . It is of note that freezing the sample for the EPR experiments in such buffer may induce a pH change to ca. pH 5.0.

2.8. Analysis of ChuS heme degradation products by HPLC and MS

H_2O_2 (2 fold molar ratio over heme) was added to 600 μM holo-ChuS in 0.1 M NaPO_4 buffer pH 7.0. After an incubation of one hour in the dark at room temperature, the protein fraction was separated from small molecular weight molecules on a 10 kDa cut-off Amicon Ultra centrifugal unit (Millipore) that had been extensively washed with NaPO_4 0.1 M pH 7.0. Both the filtrate and protein fractions were analyzed. The filtrate was lyophilized, solubilized in water and then injected on a Supelco C18 column (5 μm) equilibrated in $\text{H}_2\text{O}/0.1\%$ TFA for reverse-phase chromatography. To elute bound material, a linear gradient from 0–100% (v/v) acetonitrile in $\text{H}_2\text{O}/0.1\%$ TFA was used. The elution profile was determined using the PDA detector of an Agilent 1050 HPLC system. A compound later identified as hematinic acid by NMR spectroscopy, which showed strong absorbance at 220 nm as expected for a maleimide compound, was eluted at $\sim 20\%$ (v/v) acetonitrile. Fractions containing hematinic acid were pooled, lyophilized and solubilized in 0.1 M NaPO_4 buffer in D_2O (pD 7.4) for NMR analysis. This hematinic acid preparation was subjected to electrospray ionization mass spectrometry (ESI-MS) but the mass could not be obtained as this molecule apparently failed to ionize.

Butanol extraction of the protein fraction allowed the extraction of molecule(s) purple in color. After freeze-drying, the purple powder was solubilized in DMSO. A sample was subjected to reverse-phase chromatography on the C18 column as described above. Several of the peaks showing absorbance at 555 nm were lyophilized, dissolved in DMSO and subjected to high-resolution MS. High-resolution mass spectra were obtained with a LC/MS-TOF Agilent 6210 using electrospray

ionization (ESI). The mMass software was used to calculate theoretical mass of molecules [40].

2.9. NMR characterization of ChuS heme degradation product (hematinic acid)

A partially purified sample was lyophilized after HPLC and dissolved in 600 μL of 0.1 M NaPO_4 prepared with pure D_2O (99.9%, pD 7.4). All NMR spectra were recorded in a 5 mm tube at 20 °C on a 600 MHz INOVA spectrometer equipped with a triple resonance XYZ pulsed-field gradient probe. Assignments are based on the following NMR experiments: 1D ^1H , 2D gCOSY, 2D NOESY with 500 ms mixing time, 2D ^1H – ^{13}C HSQC and 2D ^1H – ^{13}C gHMBC with delays optimized for an 8 Hz multiple bond ^1H – ^{13}C coupling constant and a J-filter to suppress one-bond correlations. Internal DSS was used for ^1H and ^{13}C chemical shift referencing. Additional experimental details are provided in Supplementary Material (Supp. Figs. 3–6).

2.10. Quantification of released iron

The amount of iron liberated as heme was degraded by ChuS was quantified using the Prussian Blue method [41]. Samples collected 60 min after the addition of H_2O_2 to holo-ChuS were fractionated over a 10 kDa cut-off size permeation membrane (Amicon Ultra 10 K cut-off centrifugal filters). The flow-through fraction, which was free of ChuS protein as determined by SDS-Page and the absorbance at 280 nm, was used to quantify the free iron from a calibration curve prepared with FeCl_3 . A holo-ChuS sample that had not been exposed to H_2O_2 was analyzed as a negative control.

2.11. Peroxidase activity assay

Peroxidase activity of ChuS and HRP were determined spectrophotometrically using ABTS and guaiacol as substrates. Protein concentrations of 0.9 nM HRP and 1 μM holo-ChuS were used with ABTS or guaiacol at 300 μM , and H_2O_2 at 160 μM . Substrate oxidation was monitored at 415 nm for ABTS and 470 nm for guaiacol, over 30 min at 20 °C.

3. Results

3.1. The heme degrading activity of ferric ChuS is initiated by hydrogen peroxide

As shown previously [36] and here in Fig. 1 (Panel A), the ascorbate-driven heme degradation catalyzed by ChuS can be monitored by the changes in the UV–vis absorption spectrum of the heme. The optical absorption spectrum of native (ferric) holo-ChuS at pH 7.0 and in the absence of ascorbate, showed bands at 409, 549, and 586 nm (Fig. 1, panel A, black trace) that are typical for the Soret and β and α bands of a hexacoordinated low-spin (LS) heme. Upon addition of ascorbate, a clear decrease in absorbance of the heme Soret band (at 409 nm) and a concomitant appearance of a new broad band centered near 565 nm occurred over the course of 60 min. As the reaction proceeded, the absorbance in the 650–800 nm region first increased over the course of 40 min and then decreased, as indicated by the arrows (Fig. 1, panel A). The heme degradation reaction did not proceed through isosbestic points.

It is important to note that the holo-ChuS complex could be formed again by the addition of one molar equivalent of heme after the 60 min reaction as described above. Moreover, the addition of ascorbate to this newly formed complex initiated a similar heme degradation reaction (result not shown). This process could be repeated many times strongly suggesting little protein inactivation. In addition, optical spectra recorded 60 min after the initiation of each catalytic cycle showed the build-up of the species related to the distinct broad band centered at 565 nm.

Together the observations indicate that ChuS can carry several cycles of heme degradation and product(s) formation.

In canonical HOs, heme degradation is initiated by O_2 binding to the reduced heme-iron, forming the oxyferrous complex ($\text{Fe}^{\text{II}}\text{-O}_2$), which rapidly converts to ferric hydroperoxy ($\text{Fe}^{\text{III}}\text{-OOH}$) upon the addition of an electron and of a proton. This reactive species is responsible for the hydroxylation of the heme α -meso-carbon [12,27]. As such, the reaction catalyzed by HO is not inhibited by the addition of catalase since hydrogen peroxide from the solvent is not involved in the reaction [27]. In contrast to HOs, the addition of catalase (50–300 U) to a reaction containing ChuS and ascorbate slowed heme degradation activity in a concentration dependent manner, (Fig. 1A, inset). The sensitivity of the reaction catalyzed by ChuS to the presence of catalase, which was also reported for the homologous PhuS protein of *Pseudomonas* [42], strongly suggests that it was H_2O_2 , not the activation of heme-bound molecular oxygen, which initiated the heme degradation process. Without added catalase (Fig. 1A, inset), heme degradation by ChuS proceeded following a delay of several minutes. We hypothesized that this delay might constitute the time required to build sufficient levels of H_2O_2 , considering that formation of H_2O_2 could happen from O_2^- in solution. The latter would be generated by the reduction of O_2 by ascorbate through trace metal(s) from the buffer solution [43] and/or from the very fast autoxidation of the short-lived $\text{Fe}^{\text{II}}\text{O}_2$ complex of ChuS (Ouellet, Y. H. et al., in preparation). The addition of superoxide dismutase (SOD), which converts superoxide to O_2 and H_2O_2 , did not accelerate the ascorbate-driven heme degradation (data not shown) suggesting that the reaction of H_2O_2 with heme-bound ChuS was rate-limiting.

To verify this hypothesis, we monitored the synthesis of H_2O_2 in a solution of ascorbate. The results show that the addition of ChuS (1 μM and 10 μM) to an aerobic solution of ascorbate (100 μM) promoted the time-dependant formation of H_2O_2 (Fig. 1B). The rate of H_2O_2 production nearly doubled in the presence of ChuS (1 μM) and increased further at 10 μM . The amount of resulting H_2O_2 did not correlate linearly with the amount of ChuS because of its concomitant consumption by ChuS heme degradation activity (vide infra). Altogether, these results show that ChuS can accelerate the formation of H_2O_2 in an ascorbate solution. Most likely, this peroxide would be produced indirectly after the formation of superoxide and in sufficient concentrations to initiate and support its heme degradation activity.

3.2. Peroxide-driven heme degradation monitored by UV–visible electronic absorption spectroscopy

Heme degradation initiated by H_2O_2 was characterized by optical absorption spectroscopy. Immediately after the addition of H_2O_2 , the first spectrum recorded in a scanning spectrophotometer showed that the heme Soret band (409 nm) had lost intensity and the absorbance in the 650–800 nm region had increased (Fig. 2A). A stopped-flow apparatus was used to obtain the rapid-scan absorption spectra that showed the details of the fast initial event(s) of the reaction of ferric ChuS with H_2O_2 (Fig. 2B). A first transition with an apparent rate constant of 0.059 s^{-1} led to a large decrease of the Soret band and the formation of an intermediate showing absorbance in the 650–800 nm region, centered at ca. 734 nm (hence named the 734 nm species). This reaction proceeded through isosbestic points at 331, 448, 530 and 593 nm (Fig. 2B). After this initial reaction, the absorbance of the Soret band decreased further along with a disappearance of the 734 nm species in a transition with an apparent rate constant of 0.001 s^{-1} (Fig. 2B, inset). This slow transition, best observed in the scanning spectrophotometer (Fig. 2A), occurred through isosbestic points at 321, 350, 498 and 632 nm and was characterized by the appearance of the new broad band centered at 565 nm over 60 min that is referred to as the 565 nm species. It is of note that the spectral features identified during the reaction of ChuS with ascorbate, i.e. decrease of the heme Soret band with the concomitant appearance of the broad band centered at ca. 734 nm and the subsequent increase at 565 nm, were observed both

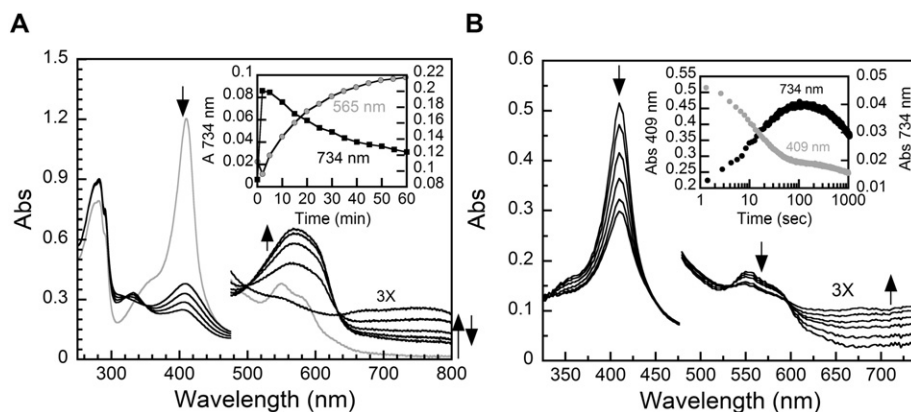


Fig. 2. Aerobic degradation of the heme of ChuS in the presence of hydrogen peroxide followed by optical absorption spectroscopy with a scanning spectrophotometer (A) and a stopped-flow apparatus (B). A – The heme degradation reaction was followed by UV-visible optical absorption spectroscopy over 60 min. H_2O_2 was added to a solution containing $10 \mu\text{M}$ ChuS in 0.1 M sodium phosphate buffer pH 7 (2:1 M ratio H_2O_2 :heme). The optical absorption spectra were recorded at regular intervals for 60 min at 20°C . The gray line represents the spectrum of ferric holo-ChuS prior to the addition of H_2O_2 . The arrows indicate the direction of the optical transitions during the course of formation of the 734 nm species and its conversion to the 565 nm species. The absorbance at 565 and 734 nm are plotted as a function of time (Inset). B – Rapid-scan electronic absorption spectra of the first 51 s of the reaction of holo-ChuS with a 2-fold excess hydrogen peroxide under aerobic conditions. The arrows indicate the direction of the optical transitions recorded in PDA mode. The inset shows the time course of the variation in absorbance at 409 nm and 734 nm (the upper limit of the PDA) over 1000 s on a logarithmic scale. These transitions were fitted to a 3 species model (ferric ChuS \rightarrow 734 nm species \rightarrow 565 nm species). The reaction was carried out at 20°C with $5 \mu\text{M}$ ferric ChuS and $10 \mu\text{M}$ hydrogen peroxide (final concentrations) in 0.1 M sodium phosphate buffer pH 7.

when using ascorbate (Fig. 1, panel A) and H_2O_2 (Fig. 2, panel A), the difference being the time scale for the appearance of the resulting species and the clear isosbestic points displayed by the peroxide-driven reaction.

It should be noted that the same rates were measured for reactions monitored by stopped-flow electronic absorption spectroscopy using white light and a PDA detector (spectra vs time data sets) or using single wavelengths and a PMT (result not shown). The latter were not due to photoreduction of heme or reaction intermediates induced by light as shown by the parallel experiments in a test tube, incubated in the dark. Clear color changes from red (ferric ChuS before the addition of hydrogen peroxide) to green (734 nm species that reached a maximal concentration at ~ 100 s) to purple (565 nm species) were observed. If left standing at room temperature for ~ 12 hours, the color of the 565 nm species evolved very slowly from purple to a pinkish (not characterized here). It is of note that the spectral transitions differed when ferric ChuS was mixed with H_2O_2 under strict anaerobic conditions. We observed a large decrease of the absorbance of the Soret band showing that the protein reacted with H_2O_2 but the 565 nm species was not observed indicating that molecular oxygen is mandatory for the above described aerobic reaction (result not shown).

As judged from the decrease of heme Soret band at 409 nm, it appears that heme degradation with H_2O_2 was slightly more complete at a 2:1 (H_2O_2 :heme) ratio than with equimolar amount (data not shown). Additionally, as expected, a large amount of heme remained intact at a ratio of 0.5:1, but the optical transition to the species absorbing at 565 nm still occurred. From these observations, we conclude that only one peroxide molecule per heme is likely used to form the transient 734 nm species and the subsequent 565 nm species. However, the 2:1 (H_2O_2 :heme) ratio was used thereafter to ensure a more complete reaction.

3.3. Pyridine complexes of reaction intermediates

To gain insight into the nature of the reaction intermediates, pyridine was added to the 734 nm species that reached a maximal concentration 100 s after the addition of a two-fold molar excess of H_2O_2 (Fig. 3). The absorption maxima detected at 395, 499, 533, 610 (sh) and 660 nm (black trace) are characteristic of those of the bis-pyridine complex of Fe^{2+} -verdoheme [26]. Using a millimolar extinction coefficient of 32.5 at 660 nm [26], we calculated that 72% of the initial heme was observed as verdoheme at this time. The formation of verdoheme, in which one meso-carbon is replaced by an oxygen atom, is fully

consistent with our reported release of CO in the reaction catalyzed by ChuS [36]. We note that the verdoheme complex formed during ChuS heme degradation is in the ferric oxidation state as revealed by the EPR spectrum (vide infra). Upon the addition of pyridine to the ChuS solution that had reacted with hydrogen peroxide, which is essentially depleted of remaining free hydrogen peroxide, an electron, possibly from an amino acid or from the solution, reduced the Fe^{3+} allowing the observation of Fe^{2+} -verdoheme-pyridine complex.

A sample collected after 60 min of reaction (565 nm species) and extracted with pyridine (gray trace) indicated that a small amount ($< 1 \mu\text{M}$) of verdoheme was still present as revealed by the peaks at 533 and 660 nm (Fig. 3). Pyridine had little effect on the wavelength maxima of the 565 nm species (wavelength maximum at 572 in pyridine) suggesting the absence of pyridine coordination. The wavelength maxima of the 565 nm species are different from those recorded for pure biliverdin in solution (373 and 668 nm) and for the biliverdin-ChuS complex (384 and 700 nm) (Supp. Fig. 2). From the lack of absorbance in the 660–700 nm region of the spectrum recorded at 60 min (565 nm species), we conclude that iron-free biliverdin was not a significant product of ChuS heme degradation. It should be pointed-out that iron-bound biliverdin (ferric biliverdin) is almost featureless in the

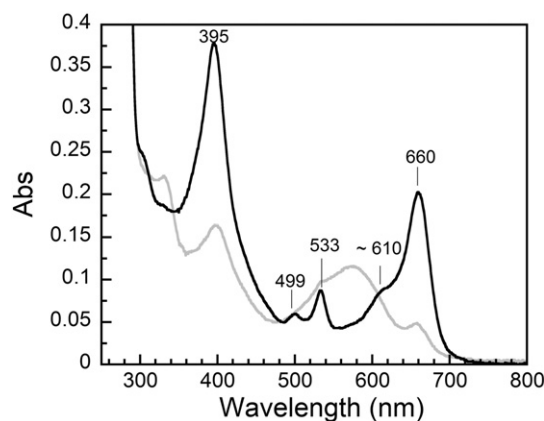


Fig. 3. Optical absorption spectra of pyridine extracts of the heme degradation reaction of ChuS with peroxide arrested at 100 s (black line) and 60 min (gray line). The samples were obtained from the reaction arrested by the addition of pyridine (16% v/v final concentration) and cleared from precipitated proteins by ultrafiltration over a 10 kDa cut-off membrane. The solution contained $10 \mu\text{M}$ holo-ChuS and $20 \mu\text{M}$ H_2O_2 .

visible region [44] and thus cannot be the origin of the strong absorption band of the 565 nm species.

3.4. Analysis of porphyrin degradation products and iron release

Samples of the 565 nm species collected after 60 min reaction of ferric ChuS with a two-fold molar excess of hydrogen peroxide were fractionated with a 10 kDa size-permeation membrane. The high-molecular weight fraction (protein fraction), contained ChuS as determined by the absorbance at 280 nm and by SDS-PAGE. The coloration of the protein fraction was purple and showed absorption maxima near 400 and 565 nm. The small molecular weight fraction was colorless but it contained a porphyrin degradation product that was detected as the heme degradation reaction was followed by NMR spectroscopy (result not shown). This substance was partially purified by reverse-phase HPLC on a C18 column and was unambiguously identified as hematinic acid using ^1H and natural abundance ^{13}C NMR spectroscopy (Fig. 4). The ^1H 1D NMR spectrum of the partially purified sample dissolved in D_2O showed only three proton resonances that could be attributed to the ChuS soluble degradation product. Resonances from impurities in the sample were identified based on significant varying ^1H intensities from samples prepared from different regions of the HPLC chromatogram. Using high resolution 1D ^1H , 2D gCOSY, 2D NOESY, 2D ^1H - ^{13}C HSQC and 2D ^1H - ^{13}C gHMBC spectra, all ^1H and ^{13}C NMR resonances were unambiguously assigned. Fig. 4 shows the assigned 2D ^1H - ^{13}C gHMBC NMR spectra of the colorless ChuS heme degradation product (the other spectra are included in Supplementary Material, Supp. Fig. 3–6). Table 1 lists all ^1H and ^{13}C chemical shifts, ^1H - ^1H coupling constants, ^1H - ^1H COSY correlations, ^1H - ^1H NOESY correlations, and long-range ^1H - ^{13}C correlations. The values and similarity of the ^{13}C chemical shifts at position C-2 (177.7 ppm) and C-5 (178.0 ppm) were used to confirm the presence of carbonyls at these positions.

Unbound iron was quantified from the small molecular weight colorless fraction. The amount of iron liberated from a reaction containing 40 μM ferric ChuS was 23.2 μM corresponding to 58%. For a reaction carried out at higher protein concentration (193 μM), only 14% of the initial heme-iron was released in solution which is consistent with the EPR detection of ChuS-bound iron (vide infra).

In addition to hematinic acid and iron found in the small molecular weight fraction, the protein fraction was successfully extracted with butanol to isolate the molecule(s) giving rise to the purple color. Analysis

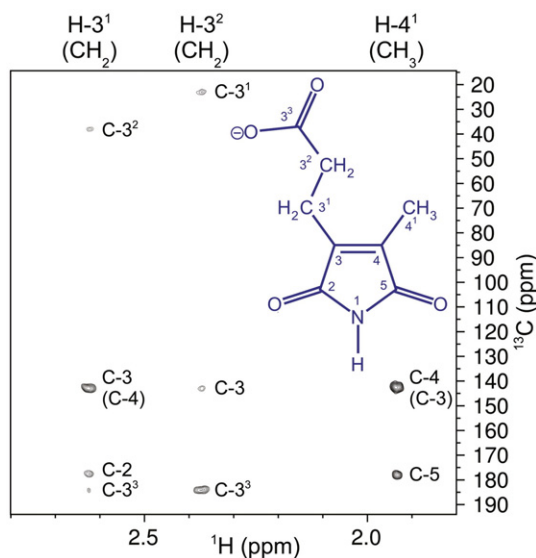


Fig. 4. 2D ^1H - ^{13}C gHMBC NMR spectra of the colorless ChuS heme degradation product partially purified by HPLC and identified as hematinic acid. Multiple bonds ^1H - ^{13}C correlations are labeled with the proton assignments above the spectra. The structure of hematinic acid is showed in blue.

of the butanol extract by reverse-phase HPLC on a C18 column afforded the observation of several peaks with absorbance in the 500–600 nm region (Fig. 5A–B). Analysis by high-resolution electrospray ionization mass spectrometry (ESI-MS) of peaks b–d displaying the highest level of absorbance at 555 nm revealed a mass of 437.1913 m/z (Supp. Fig. 5C). Based on mass and composition of the starting heme (protoporphyrin IX, $\text{C}_{34}\text{H}_{34}\text{N}_4\text{O}_4$, $[\text{M} + 1\text{H}]^{1+}$ 563.2653 m/z), the 437.1913 m/z indicates a $\text{C}_{24}\text{H}_{26}\text{N}_3\text{O}_5$ molecule with an error of -0.0032 between the observed and the calculated $[\text{M} + 1\text{H}]^{1+}$ mass. This represents a net loss of 10 C, 8 H, 1 N and the gain of 1 O compared to heme (protoporphyrin IX). Protoporphyrin IX contains 4 pyrroles and hematinic acid ($\text{C}_8\text{H}_9\text{NO}_4$) contains only one. The molecule(s) with 437.1913 m/z is consistent with the cleavage of protoporphyrin IX at two adjacent meso carbons and the formation of a tripyrrole product(s) containing both vinyl groups and one propionate group (Fig. 5D).

3.5. Peroxide-driven heme degradation monitored by EPR spectroscopy

Low temperature EPR spectroscopy was used to further characterize the electronic structure of the different species formed when mixing ferric ChuS with hydrogen peroxide in aerobic conditions. Fig. 6 shows the 9-GHz EPR spectra, recorded at 4 K, of ferric ChuS in the resting state (black trace, bottom) and after reaction with hydrogen peroxide (green and dark red traces, top). The holo-ChuS EPR spectrum (black trace) is typical for heme iron in the ferric oxidation state, showing contributions of both high-spin (HS) and low-spin (LS) EPR signals, with effective g -values of $g_{\perp} = 6.01$ and $g_{\parallel} = 1.99$ for the HS signal and of $g_1 = 2.85$, $g_2 = 2.16$ and $g_3 = 1.70$ for the LS signal. The relative contribution of the HS and LS spin species were shown to be pH dependent (results not shown). Mixing the ferric ChuS protein with 2-folds excess H_2O_2 at room temperature and for 10 s (before freezing the samples) resulted in a dramatic decrease (90% conversion) in intensity of the ferric HS signal, the complete disappearance of the ferric LS signal, and concomitant appearance of three new EPR signals, labeled A, B and C in Fig. 6 (green trace). The narrow Signal A at $g^A = 2.00$ (Fig. 6, inset) agrees well with a ferrous keto π neutral radical, one of the three resonance structures of the α -meso-hydroxyheme² previously characterized as intermediate in the heme degradation process of heme oxygenases [45]. Signal B, with g -values of 2.50, 2.12 and 1.87 (Fig. 6, inset) is virtually identical to the rhombic LS EPR signal of ferric verdoheme, also previously reported for heme oxygenases [22,45]. Signal C, with a strong resonance at $g^C = 4.29$ and a much weaker one at $g = 9.58$ is consistent with a non-heme HS ($S = 5/2$) ferric iron being in a rhombically distorted coordination environment as shown for the mononuclear iron site in *Trepionema pallidum* nearedoxin [46] or one of the mononuclear iron centers in *Desulfovibrio desulfuricans* desulfoferrodoxin [47]. It is of note that the apparent difference in yield for the three species is due to the fact that they have very different relaxation properties, hence the signals, Signals A and B, are somewhat saturated (that is the observed intensity is reduced) in the experimental conditions used to record the spectra (temperature, 4 K and microwave power, 1 mW), unlike the resting ferric ChuS and the non-heme iron (Signal C). The same three new EPR signals (labeled A, B and C) were observed when mixing ChuS and hydrogen peroxide up to 60 s at room temperature.

Based on the kinetics of the different species shown by the stopped-flow UV-vis absorption experiments (Fig. 2), we used the approach of mixing at lower temperatures in order to slow down the reaction, and possibly detect changes in the relative intensities of the three signals contributing to the EPR spectrum. Accordingly, when ferric ChuS was mixed with H_2O_2 on ice and during 2 s (Fig. 6, dark red trace) less conversion of the ferric EPR signals was observed, with the concomitant

² For HO-1, the hydroxylated meso-carbon of the hydroxyheme complex is at position α . For ChuS, it was not determined which meso-carbon is hydroxylated.

Table 1
Identification by NMR of hematinic acid released as a soluble product of heme degradation by ChuS.

#	δ ^1H (ppm)	^1H – ^1H coupling (Hz)	δ ^{13}C (ppm)	^1H – ^1H correlations (ppm)	^1H – ^{13}C HMBC correlations (ppm)
3 ¹ (CH ₂)	2.63	7.6 (³ J, 3 ¹ –3 ²) 0.96 (³ J, 3 ¹ –4 ¹)	22.8	COSY: 2.37(s), 1.93(w) NOESY: 1.94(w), 2.36(m)	38.0, 143.0, 177.7, 184.2
3 ² (CH ₂)	2.37	7.6 (³ J, 3 ² –3 ¹)	38.1	COSY: 2.63(s) NOESY: 2.64(m)	23.0, 143.0, 184.1
4 ¹ (CH ₃)	1.93	0.84 (⁵ J, 4 ¹ –3 ¹)	10.6	COSY: 2.63(w) NOESY: 2.62(w)	142.6, 178.0
2	–	–	177.7	–	–
3	–	–	143.0	–	–
4	–	–	142.6	–	–
5	–	–	178.0	–	–
3 ³	–	–	184.1	–	–

NMR data acquired at ^1H frequency of 600 MHz and at 20 °C. Chemical shifts referenced to internal DSS. (s), (m) and (w) indicate strong, medium and weak correlations, respectively. The long-range ^5J coupling constant was measured from a high resolution 1D spectrum (Supp. Fig. 3). ^{13}C chemical shifts for carbons 3¹, 3² and 4¹ were obtained from a ^1H – ^{13}C HSQC (Supp. Fig. 4). ^{13}C chemical shifts for carbons 2, 3, 4, 5 and 3³ were obtained from a ^1H – ^{13}C HMBC (Fig. 5). 2D gCOSY and NOESY spectra are shown in Supp. Figs. 5 and 6, respectively.

lower intensity of the three signals, in particular that of Signal B as compared to the Signal A. But, when using 10 s mixing time on ice, the spectra obtained was virtually identical to that of the room-temperature mixing case (Fig. 6, green trace), described above. More importantly, the relative ratio of Signals A and B is reversed in the 10 s mixing-time spectrum (Fig. 6, green trace) as compared to the 2 s mixing-time case (Fig. 6, dark red trace), hence showing that the ferrous keto π neutral radical (resonance structures of the *meso*-hydroxyheme, Signal A) precedes the ferric verdoheme (Signal B) and the bound ferric iron species (Signal C).

Accordingly, the sequential disappearance and appearance of the signals contributing to the EPR spectrum of ChuS upon mixing with H₂O₂ are consistent with those observed in the absorption spectra (Fig. 2). Specifically, a band observed at ca. 800 nm was previously reported as the α -*meso*-hydroxyheme species for HO [45]. The ferric verdoheme intermediate formed in HO was reported to have an absorption band ranging from 600 to 700 nm, and centered at ca. 680 nm [45]. In the case of ChuS, the ferric verdoheme band would overlap with that of *meso*-hydroxyheme resulting in the observed broad band in the 650–800 nm region (the 734 nm species) and consistent with the EPR Signals

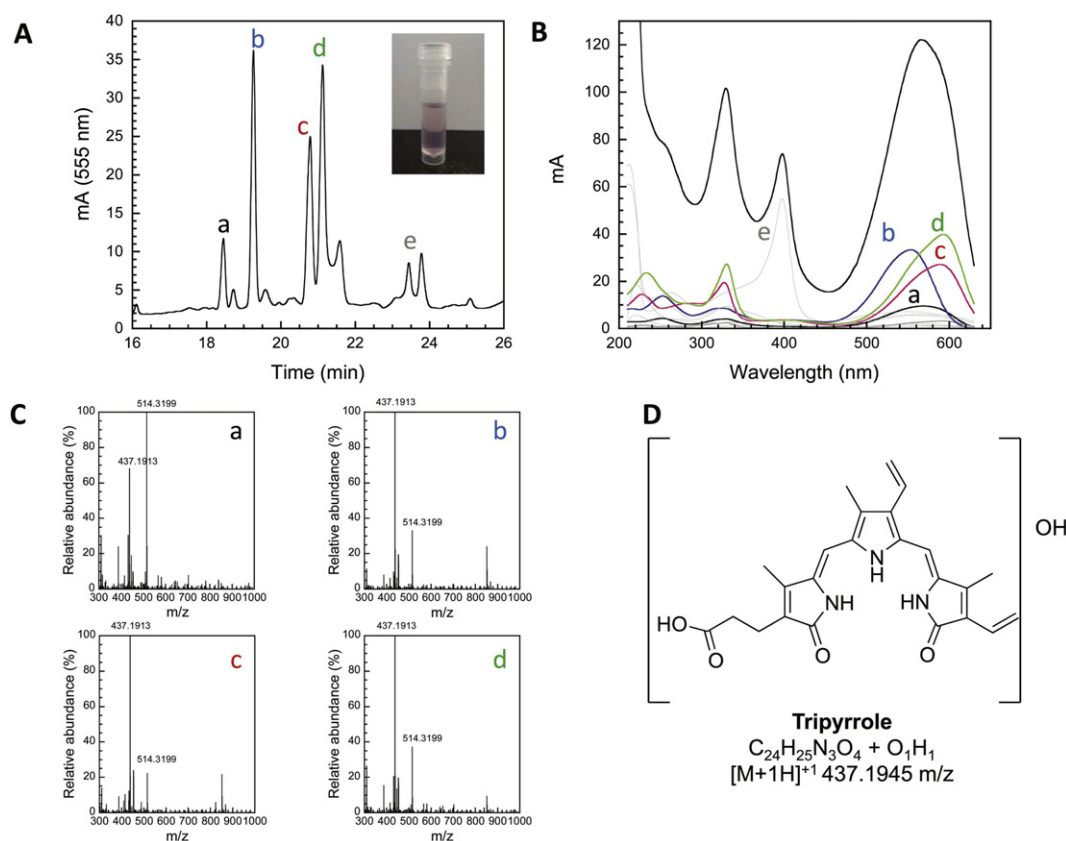


Fig. 5. HPLC and MS analysis of the butanol-solubilized ChuS heme degradation product(s). **A** – Porphyrin degradation product(s) that remained bound to ChuS following heme degradation by H₂O₂ for 60 min were extracted with butanol. The HPLC profile of the butanol extract on a C18 column is shown at 555 nm. A picture of the butanol extract prior to HPLC is shown as an inset. **B** – Optical absorption spectra recorded at the peaks of the HPLC chromatogram shown in **A**. The spectra of the most intense peaks are shown in black (peak a), blue (peak b), red (peak c) and green (peak d) while the less intense ones are shown in gray. The top black line is the calculated spectrum of the mixture obtained by adding all the spectra. Peak e corresponds to undegraded porphyrin (heme). **C** – High-resolution ESI-MS profiles of peaks a-d. **D** – Proposed structure of a tripyrrole molecule consistent with the 437.1913 m/z. The calculated mass indicates that one more oxygen and hydrogen atoms would be present on the molecule unless these additional masses originated from the ionization process. The tripyrrole shown is drawn from cleavage at the β and γ *meso*-carbons. It was not determined here if cleavage occurred at these *meso*-carbons or if it occurred at the γ and δ *meso* carbons of the heme.

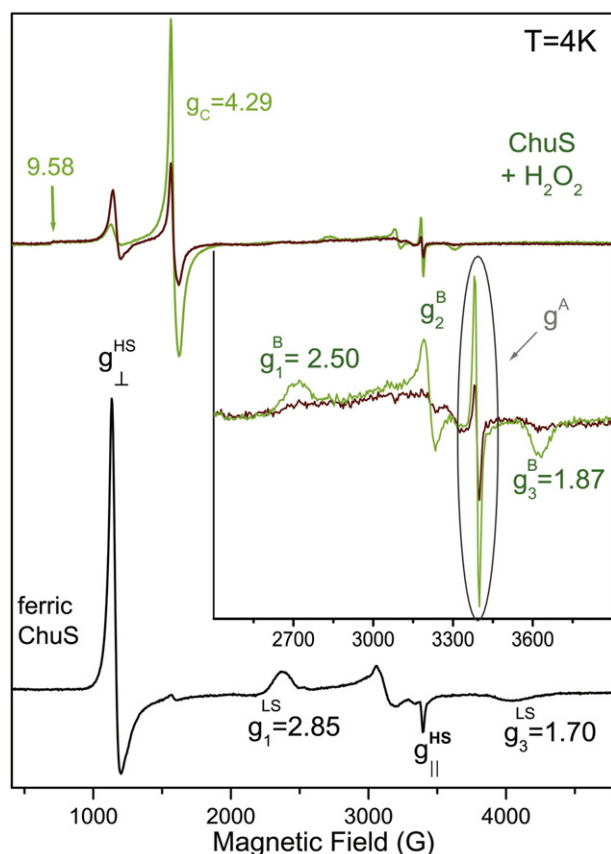


Fig. 6. The 9-GHz EPR spectra of ferric ChuS (black trace) and upon reaction with 2-fold excess hydrogen peroxide, at 20 °C for 10 s (green trace) or at 2 °C for 2 s (dark red trace). Inset: enlargement of the spectral region where the ferrous keto π -neutral radical (Signal A) and the ferric verdoheme (Signal B) intermediates are detected. Experimental conditions: T = 4 K, 5G modulation amplitude, 1 mW microwave power, 100 kHz modulation frequency. The ferric ChuS sample (heme) concentration used was 0.67 mM, in phosphate buffer pH 7.0.

A and B, assigned to the *meso*-hydroxyheme and ferric verdoheme, respectively. The broad band (500–650 nm) of the 565 nm species in the absorption spectrum, that was identified as a porphyrin degradation product (tripyrrole) by the MS and NMR experiments, would also overlap with the contribution of non-heme iron (Signal C) [46,47] detected in the EPR spectrum.

3.6. Peroxidase activity

We examined whether ferric ChuS could use H_2O_2 to oxidize ABTS and guaiacol in a reaction analogous to that of peroxidases. No detectable substrate oxidation could be measured for ChuS, even at a high protein concentration (1 μ M) in contrast to the easily detected oxidation of ABTS by nM concentration of HRP (data not shown). These results strongly suggest that in the presence of H_2O_2 , ferric ChuS does not form the high-valent intermediate(s) that react with substrates in a peroxidase-like mechanism [48]. Hence H_2O_2 is apparently used by ChuS exclusively for its own heme degradation activity.

4. Discussion

ChuS is a protein encoded by a gene of the *chu* gene cluster involved in heme internalization in *E. coli* O157:H7. We have previously shown that recombinant ChuS degrades heme and releases CO in a reaction mediated by ascorbate or NADPH and cytochrome P450 reductase [36,

37]. Our present results reveal that the substrates of this reaction are not electrons and oxygen, as expected for a canonical HO, but hydrogen peroxide that is formed in solution in the presence of ascorbate and O_2 and is accelerated by ChuS. This explains the delay in the initiation of the heme degradation reaction using ascorbate. The overall ascorbate-driven reaction and the peroxide-driven reaction seem to proceed through similar optical transitions (Figs. 1 and 2). However, unlike the ascorbate-driven reaction, the reaction of ferric ChuS with H_2O_2 starts without delay and produces distinct optical transitions that proceed through isosbestic points suggesting the formation of intermediate species. We thus characterized the details of the reaction of ChuS with hydrogen peroxide using optical absorption and EPR spectroscopies to gain a better understanding of the electronic structures of the intermediate species formed in the course of reaction and thus, a better understanding of the reaction mechanism. Porphyrin degradation products were identified by MS and NMR spectroscopy.

It is of note that both LS and HS forms of the resting ferric heme of ChuS were reactive upon addition of H_2O_2 , as shown by the nearly complete disappearance of the corresponding EPR signals and the concomitant appearance of the three new and distinct EPR signals (Fig. 6, green trace), thus indicating that the LS signal does not arise from a nitrogenous axial ligand on the heme distal side. The g -values of the LS ferric form for the resting holo-ChuS ($g_1 = 2.85$, $g_2 = 2.16$, $g_3 = 1.70$) are consistent with the presence of a water molecule close to the iron on the heme distal side, and most possibly in H-bond interactions to a nitrogenous species [49]. Interestingly, a water molecule is observed in the crystal structure of the homologous HemS protein of *Yersinia enterocolitica* [50] and was suggested as the sixth axial ligand of the homologous PhuS protein of *P. aeruginosa* based on spectroscopic evidence [42]. In the ChuS structure, a formate molecule from the crystallization buffer [37] has been observed, possibly replacing the native water molecule. Then, the N from Arg 100 would be in H-bonding distance and in agreement with the EPR spectrum (see above).

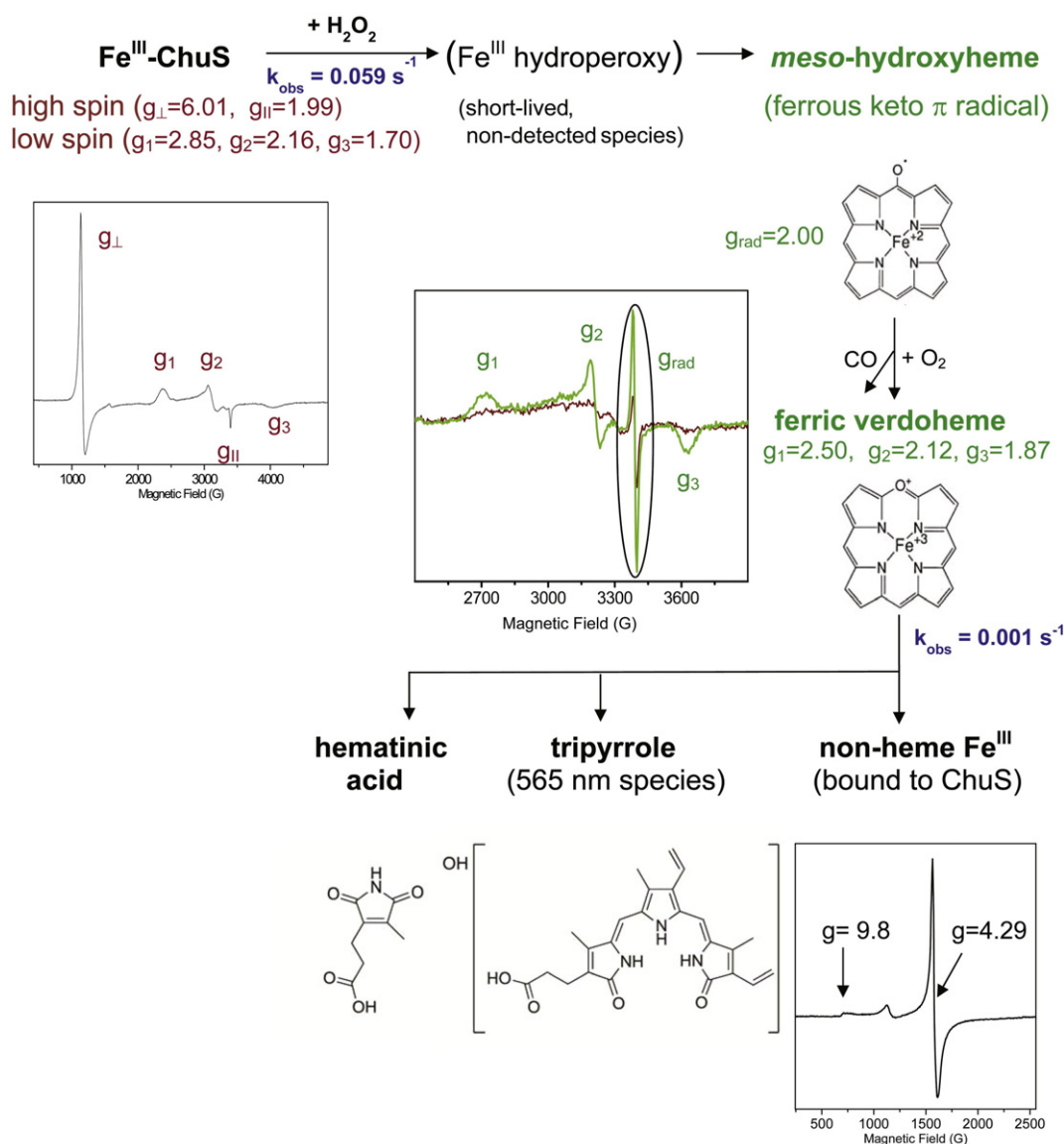
In the case of the well-characterized heme oxygenases, the initial step for O_2 activation is the formation of the ferric hydroperoxy species ($Fe^{III}-OOH$) resulting from the activation of the $Fe^{II}O_2$ complex or from the reaction with H_2O_2 (for a recent review, see [12]). Such intermediate is rather short-lived, hence it could only be characterized applying the cryoreduction approach to an oxy-HO sample [20]. The EPR spectrum of the $Fe^{III}-OOH$ showed a LS ferric signal with g -values of $g_1 = 2.31$, $g_2 = 2.18$ and $g_3 = 1.92$. In the case of ChuS, both EPR signals of LS species detected before and after addition of hydrogen peroxide (see Fig. 6) show very different g -values to those expected for a ferric hydroperoxy species. Accordingly, the ferric hydroperoxy species in ChuS is concluded to be as transient as in the case of HO. In contrast, the species related to the subsequent step in heme oxygenation (i.e. *meso*-hydroxylation) proved to be longer-lived in ChuS as compared to HO, since it could be trapped by manual mixing and characterized by EPR spectroscopy (Signal A in Fig. 6). An intriguing difference between ChuS and HO is that the ferrous keto π -neutral radical species could only be detected during the anaerobic reaction of HO with hydrogen peroxide [45], and converted readily to the ferric verdoheme intermediate when exposed to O_2 [22, 45]. The difference in stability of the ferrous keto π -neutral radical species formed in ChuS could be explained by differences in the electronic properties of the heme within the binding site. It is of note that we can rule out a protein-based radical species ($g \approx 2$) as the origin of the EPR Signal A, based on its relaxation properties but also on the fact that no peroxidase-like activity of ChuS could be detected when mixing ChuS with H_2O_2 in the presence of typical peroxidase substrates (see Section 3.6).

The other EPR signal detected for ChuS upon reaction with hydrogen peroxide was that of a LS ferric heme having g -values of $g_1 = 2.50$, $g_2 = 2.12$, and $g_3 = 1.87$ (Fig. 6), consistent with a ferric verdoheme intermediate. Our low temperature EPR experiments (see Results Section 3.5) clearly showed that the formation of the ferrous keto π -neutral radical and the ferric verdoheme species

were sequentially correlated, as judged by the changes in the relative intensity of the EPR signals (see Fig. 6).

Last but not least, the predominant EPR signal with g -values of $g = 4.29$ and $g = 9.58$ that is entirely consistent with a non-heme HS Fe^{III} in a rhombically distorted coordination environment, clearly indicated that the final step of the reaction of ChuS with H_2O_2 and O_2 involves the release of the ferric iron, a fraction of which binds to the protein. Moreover, the analysis of the products by MS and NMR showed that a tripyrrole, and hematinic acid, represented in Figs. 4 and 5D, are the degradation products of the heme degradation reaction that released the iron. The specific mechanism by which the ferric iron is released in ChuS, i.e. the cleavage of the porphyrin, is under study. The g -values of the EPR signal from ferric non-heme iron detected in ChuS strongly indicated that at the protein concentration used to follow the reaction by EPR, most of the released iron is not free iron in solution, but coordinated with predominantly nitrogenous and/or oxygenous ligands [47]. It is not possible to assess so far the binding site for the non-heme iron and whether it is specific one or the iron just binds to the protein surface.

Based on the present initial characterization and identification of the different species involved in the aerobic reaction of holo-ChuS with hydrogen peroxide, we propose a tentative scheme with the different reaction steps (Scheme 1) inspired by the well-characterized species involved in the activation of dioxygen by canonical HOs and the peroxide-shunt pathway. ChuS appears to share with HOs the ability to carry out the modification of the heme to meso-hydroxyheme when it reacts with peroxide (peroxide-shunt pathway). The unequivocal identification of ferric verdoheme as an intermediate by its EPR spectrum, and from the distinct optical absorption spectrum of the ferrous verdoheme complex with pyridine, is consistent with the requirement of molecular oxygen for the H_2O_2 -driven reaction with ChuS. This evidence supports our proposal in Scheme 1 for a reaction proceeding via the formation of verdoheme from meso-hydroxyheme. With rat HO1, the reaction of ferric heme with an equimolar amount of peroxide was shown to be arrested at the verdoheme stage. Only with addition of cytochrome P450 reductase and NADPH did the reaction continue to biliverdin [51]. In contrast, the reaction of ferric ChuS with H_2O_2 is not



Scheme 1. Reaction pathways for the reaction of ChuS with hydrogen peroxide. The native (resting) ChuS (black trace) and intermediates of the reaction with hydrogen peroxide (red and green traces) identified by their EPR spectra as well as the heme degradation products identified by NMR spectroscopy (hematinic acid) and HPLC/MS (tripyrole) are shown. The ferrous keto- π -radical species detected by EPR spectroscopy ($g_{\text{rad}} = 2.00$) is one of the resonance structures of the meso-hydroxyheme intermediate. The observed kinetic constants (s^{-1}) obtained from the rapid-scan electronic absorption spectrum of the reaction of ChuS with hydrogen peroxide are also shown (in blue).

arrested at the verdoheme stage but proceeds further to release ferric iron that partially binds to the protein (Scheme 1).

The simple hydrolytic cleavage of the porphyrin ring from verdoheme would produce biliverdin [52]. As judged from the optical spectrum of products after 60 min of incubation of holo-ChuS with peroxide, iron-free biliverdin does not appear to be a significant heme degradation product by ChuS. Rather, hematinic acid, which contains one pyrrole, was identified as a porphyrin degradation product along with the remaining portion of the porphyrin, which is a tripyrrole compound (Scheme 1). The mechanism by which a second meso-carbon is attacked leading to the release of hematinic acid from verdoheme remains to be established. In this context, it is interesting that a synthetic ferric oxaphlorin, a porphyrin with a carbonyl group at a meso-carbon, was shown to be oxidized by O₂ without the addition of reductant when incubated in pyridine [53–55]. This reaction led to the release of one of the pyrrole by an as yet undetermined mechanism. A similar oxygen-dependant reaction cleaving the verdoheme at adjacent meso carbons and releasing hematinic acid and a tripyrrole may be facilitated within the environment of the ChuS protein. In such as case, molecular oxygen would be required for heme degradation by ChuS both at the conversion of meso-hydroxyheme to verdoheme step and at the opening of the porphyrin ring at adjacent meso-carbons step. This scenario is consistent with the absence of formation of the tripyrrole under strict anaerobic condition. Although the reaction leading to the formation of the tripyrrole appears to be quite slow, we suspect that it may be modulated within the bacterial cell by other proteins or small molecules. We also did not investigate here if the cleavage of the ChuS-bound verdoheme would be accelerated with additional reductant.

Biliverdin, hematinic acid and various mono-, di- and tripyrrole molecules are known to be formed by chemical oxidation of heme under strong oxidizing conditions, a process known as coupled heme oxidation. In the coupled oxidation reaction, the reduced or the oxygenated state of heme proteins reacts with hydrogen peroxide resulting in degraded heme [56,57]. The novelty of our findings related to the ChuS-mediated reaction is that hematinic acid and the tripyrrole molecule(s) are formed from the ferric oxidation state of the heme and under relatively mild conditions, i.e. stoichiometric concentration of peroxide. In addition to the well characterized HO, that produces biliverdin [11–14,16], the IsdG family of proteins found in Gram-positive bacteria is known to degrade heme to oxo-biliverdins [33] and recently, the MhuD enzyme from another Gram-positive bacterium, *Mycobacterium tuberculosis*, was shown to synthesize mycobilins [34]. Overall, the heme degradation reaction shown here by ChuS provides a first

example of heme degradation by a protein not homologous to HO in Gram-negative bacterium that degrades heme to products that are not biliverdin. It also constitutes another example of the expanding repertoire of reactions catalyzed by heme degrading enzymes.

Different functions have been described for the ChuS family of proteins. The homologous PhuS from *Pseudomonas* has been the most characterized. ChuS and PhuS share a somewhat high degree of sequence identity for each other (38% identity) and for other members of the family (Fig. 7), in both the C-terminal-flanked heme containing domain and the N-terminal-flanked domain that is devoid of heme, as well as an overall conserved three-dimensional structures [36,37,58,59]. Evidence from biochemical studies and in vivo experiments support the proposal that PhuS acts as a chaperone that transfers heme to the canonical HO (HemO) that is present in this bacterium [42,60–63]. In absence of the *phuS* gene, heme utilization is not optimal and the bacteria secrete less biliverdin, the product as of the activity of the canonical heme hemO, in the growth medium [64]. The ability of PhuS itself to degrade heme was investigated and it appears to be limited to the conversion of heme to verdoheme [42,59]. The specific heme environment of these proteins likely plays a large role in this different outcome [59]. To date, no canonical HO has been identified in any strain of *E. coli*. The fact that ChuS can release the Fe from heme suggests that ChuS could be beneficial for the survival and growth of the pathogenic *E. coli* O157:H7 under iron-limited condition, and possibly of other bacteria that possess homologs of this protein, in the absence of a canonical HO. However, it should be kept in mind that other functions are possible. In addition to the chaperone activity proposed for PhuS, a protective role from oxidative stress was also proposed for this family of proteins [65–67]. The fact that ChuS contributes to the generation of H₂O₂ in solution and that it reacts with H₂O₂ in the low-micromolar range suggests that it could also be involved in the oxidative-stress response of *E. coli* O157:H7.

Acknowledgments

We thank Prof. Normand Voyer and François Otis for the use of their HPLC system and their help with the purification of ChuS heme degradation products and the department of chemistry, especially Pierre Audet, for the analysis by ESI-mass spectrometry. We also thank Prof. Michel Guertin for insightful discussions. This work was supported by NSERC discovery grant 250073 to M.C.. A.I. acknowledges financial support from CNRS and CEA-Saclay, and the France–Quebec Cooperation

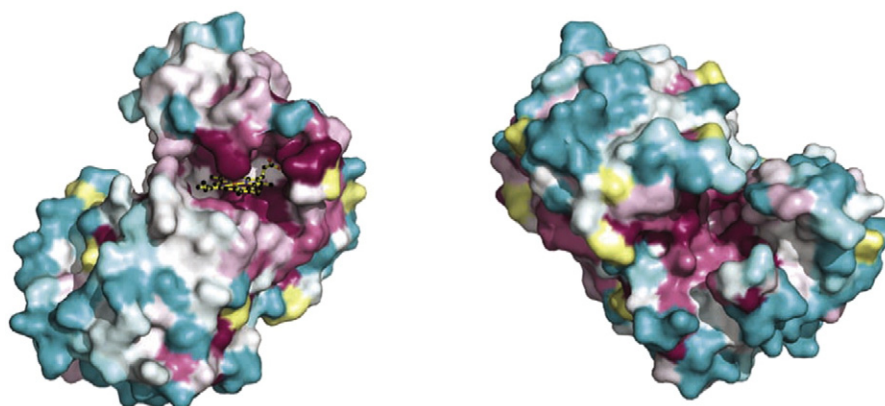


Fig. 7. Phylogenetic mapping of homologous sequences to the ChuS architecture. Structural characterization of ChuS showed that it is composed of a structural repeat linked by a long segment of bridging residues [36]. Although they share the same topology, the N- and C-terminal halves of ChuS share only 19% sequence identity. ChuS homologs are found in a wide range of proteobacteria [50]. Similarly to Schneider et al., we identified 266 homologous sequences to ChuS by Blastp and Blast explorer analysis include representative proteins from a diverse group of bacterial species including representatives from *Escherichia*, *Shigella*, *Citrobacter*, *Enterobacter*, *Yersinia*, *Serratia*, *Klebsiella*, and *Pseudomonas*, many of which are prolific human pathogens. Conserved residues are shown in pink, neutral in white, ambiguous in yellow, and non-conserved in blue as per ConSurf standard coloration scheme [68]. The H193 binding site of ChuS complex with heme (left) and the mirror site (right) are highly conserved, indicating that the mirror site is not an artifact of the suspected gene duplication event that formed ChuS [36,37].

Program PEES (2011–2012) #63.127 for a visiting stipend and Z.J. acknowledges the grant support from CIHR (MOP-48370).

Appendix A. Supplementary data

Supplementary data to this article can be found online at <http://dx.doi.org/10.1016/j.jinorgbio.2015.11.002>.

References

- [1] J.P. McHugh, F. Rodriguez-Quinones, H. Abdul-Tehrani, D.A. Svistunenko, R.K. Poole, C.E. Cooper, S.C. Andrews, *J. Biol. Chem.* 278 (2003) 29478–29486.
- [2] H. Budzikiewicz, in: P. Cornelis, S.C. Andrews (Eds.), *Iron Uptake and Homeostasis in Microorganisms*, Caister Academic Press, Norfolk 2010, pp. 1–16.
- [3] C. Wandersman, in: P. Cornelis, S.C. Andrews (Eds.), *Iron Uptake and Homeostasis in Microorganisms*, Caister Academic Press, Norfolk 2010, pp. 17–36.
- [4] H. Pennington, *Lancet* 376 (2010) 1428–1435.
- [5] J.Y. Lim, J. Yoon, C.J. Hovde, *J. Microbiol. Biotechnol.* 20 (2010) 5–14.
- [6] D. Law, J. Kelly, *Infect. Immun.* 63 (1995) 700–702.
- [7] E.E. Wyckoff, D. Duncan, A.G. Torres, M. Mills, K. Maase, S.M. Payne, *Mol. Microbiol.* 28 (1998) 1139–1152.
- [8] A.G. Torres, S.M. Payne, *Mol. Microbiol.* 23 (1997) 825–833.
- [9] E.C. Hagan, H.L. Mobley, *Mol. Microbiol.* 71 (2009) 79–91.
- [10] I. Stojiljkovic, K. Hantke, *Mol. Microbiol.* 13 (1994) 719–732.
- [11] T. Matsui, M. Iwasaki, R. Stugiyama, M. Unno, M. Ikeda-Saito, *Inorg. Chem.* 49 (2010) 3602–3609.
- [12] T. Matsui, M. Unno, M. Ikeda-Saito, *Acc. Chem. Res.* 43 (2010) 240–247.
- [13] A. Wilks, G. Heinzl, *Arch. Biochem. Biophys.* 544 (2014) 87–95.
- [14] P.R.O. de Montellano, *Curr. Opin. Chem. Biol.* 4 (2000) 221–227.
- [15] D.R. Benson, M. Rivera, *Met. Ions Life Sci.* 12 (2013) 279–332.
- [16] M. Rivera, J.C. Rodriguez, *Met. Ions Life Sci.* 6 (2009) 241–293.
- [17] P.R.O. de Montellano, *Curr. Opin. Chem. Biol.* 4 (2000) 221–227.
- [18] S. Takahashi, K. Ishikawa, N. Takeuchi, M. Ikeda-Saito, T. Yoshida, D.L. Rousseau, *J. Am. Chem. Soc.* 117 (1995) 6002–6006.
- [19] M. Unno, T. Matsui, G.C. Chu, M. Couture, T. Yoshida, D.L. Rousseau, J.S. Olson, M. Ikeda-Saito, *J. Biol. Chem.* 279 (2004) 21055–21061.
- [20] R.M. Davydov, T. Yoshida, M. Ikeda-Saito, B.M. Hoffman, *J. Am. Chem. Soc.* 121 (1999) 10656–10657.
- [21] S. Takahashi, K.M. Matera, H. Fujii, H. Zhou, K. Ishikawa, T. Yoshida, M. Ikeda-Saito, *D.L. Rousseau, Biochemistry* 36 (1997) 1402–1410.
- [22] H. Sakamoto, Y. Omata, G. Palmer, M. Noguchi, *J. Biol. Chem.* 274 (1999) 18196–18200.
- [23] C.O. Damaso, R.A. Bunce, M.V. Barybin, A. Wilks, M. Rivera, *J. Am. Chem. Soc.* 127 (2005) 17582–17583.
- [24] L. Lad, P.R.O. de Montellano, T.L. Poulos, *J. Inorg. Biochem.* 98 (2004) 1686–1695.
- [25] M. Unno, T. Matsui, M. Ikeda-Saito, *J. Inorg. Biochem.* 113 (2012) 102–109.
- [26] H. Sakamoto, Y. Omata, Y. Adachi, G. Palmer, M. Noguchi, *J. Inorg. Biochem.* 82 (2000) 113–121.
- [27] M. Rivera, Y. Zeng, *J. Inorg. Biochem.* 99 (2005) 337–354.
- [28] A. Wilks, M.P. Schmitt, *J. Biol. Chem.* 273 (1998) 837–841.
- [29] C.A. Kunkle, M.P. Schmitt, *J. Bacteriol.* 189 (2007) 3650–3654.
- [30] D.J. Schuller, W. Zhu, I. Stojiljkovic, A. Wilks, T.L. Poulos, *Biochemistry* 40 (2001) 11552–11558.
- [31] W. Zhu, A. Wilks, I. Stojiljkovic, *J. Bacteriol.* 182 (2000) 6783–6790.
- [32] M. Ratliff, W. Zhu, R. Deshmukh, A. Wilks, I. Stojiljkovic, *J. Bacteriol.* 183 (2001) 6394–6403.
- [33] M.L. Reniere, G.N. Ukpabi, S.R. Harry, D.F. Stec, R. Krull, D.W. Wright, B.O. Bachmann, M.E. Murphy, E.P. Skaar, *Mol. Microbiol.* 75 (2010) 1529–1538.
- [34] S. Nambu, T. Matsui, C.W. Goulding, S. Takahashi, M. Ikeda-Saito, *J. Biol. Chem.* 288 (2013) 10101–10109.
- [35] A. Wilks, M. Ikeda-Saito, *Acc. Chem. Res.* (2014).
- [36] M.D. Suits, G.P. Pal, K. Nakatsu, A. Matte, M. Cygler, Z. Jia, *Proc. Natl. Acad. Sci. U. S. A.* 102 (2005) 16955–16960.
- [37] M.D. Suits, N. Jaffer, Z. Jia, *J. Biol. Chem.* 281 (2006) 36776–36782.
- [38] C.A. Appleby, *Methods Enzymol.* 52 (1978) 157–166.
- [39] R.W. Noble, Q.H. Gibson, *J. Biol. Chem.* 245 (1970) 2409–2413.
- [40] M. Strohal, M. Hassman, B. Kosata, M. Kodicek, *Rapid Commun. Mass Spectrom.* 22 (2008) 905–908.
- [41] S. Boutry, D. Forge, C. Burtea, I. Mahieu, O. Murariu, S. Laurent, L. Vander Elst, R.N. Muller, *Contrast Media Mol. Imaging* 4 (2009) 299–304.
- [42] I.B. Lansky, G.S. Lukat-Rodgers, D. Block, K.R. Rodgers, M. Ratliff, A. Wilks, *J. Biol. Chem.* 281 (2006) 13652–13662.
- [43] G.R. Buettner, *Free Radic. Res. Commun.* 1 (1986) 349–353.
- [44] Y. Liu, P.R.O. de Montellano, *J. Biol. Chem.* 275 (2000) 5297–5307.
- [45] Y. Liu, P. Moenne-Loccoz, T.M. Loehr, P.R. Ortiz de Montellano, *J. Biol. Chem.* 272 (1997) 6909–6917.
- [46] T. Jovanovic, C. Ascenso, K.R.O. Hazlett, R. Sikkink, C. Krebs, R. Litwiller, L.M. Benson, I. Moura, J.J.G. Moura, J.D. Radolf, B.H. Huynh, S. Naylor, F. Rusnak, *J. Biol. Chem.* 275 (2000) 28439–28448.
- [47] P. Tavares, N. Ravi, J.J.G. Moura, J. Legall, Y.H. Huang, B.R. Crouse, M.K. Johnson, B.H. Huynh, I. Moura, *J. Biol. Chem.* 269 (1994) 10504–10510.
- [48] G. Smulevich, A. Feis, B.D. Howes, A. Ivancich, in: K.M. Kadish, K.M. Smith, R. Guilard (Eds.), *Handbook of Porphyrin Science*, vol. 6, World Scientific, Hackensack, N. J., 2010 (Chap. 31).
- [49] A.I. Celis, Z. Geeraerts, D. Ngmenterebo, M.M. Machovina, R.C. Kurker, K. Rajakumar, A. Ivancich, K.R. Rodgers, G.S. Lukat-Rodgers, J.L. DuBois, *Biochemistry* 54 (2015) 434–446.
- [50] S. Schneider, K.H. Sharp, P.D. Barker, M. Paoli, *J. Biol. Chem.* 281 (2006) 32606–32610.
- [51] A. Wilks, P.R. Ortiz de Montellano, *J. Biol. Chem.* 268 (1993) 22357–22362.
- [52] S. Saito, H.A. Itano, *Proc. Natl. Acad. Sci. U. S. A.* 79 (1982) 1393–1397.
- [53] S.P. Rath, M.M. Olmstead, L. Latos-Grazynski, A.L. Balch, *J. Am. Chem. Soc.* 125 (2003) 12678–12679.
- [54] A.L. Balch, F.L. Bowles (Eds.), *Coordination Chemistry of Verdohemes and Open-Chain Oligopyrrole Systems Involved in Heme Oxidation and Porphyrin Destruction*, World Scientific Publishing Co, 2010.
- [55] S.P. Rath, H. Kalish, L. Latos-Grazynski, M.M. Olmstead, A.L. Balch, *J. Am. Chem. Soc.* 126 (2004) 646–654.
- [56] L. Avila, H.W. Huang, C.O. Damaso, S. Lu, P. Moenne-Loccoz, M. Rivera, *J. Am. Chem. Soc.* 125 (2003) 4103–4110.
- [57] J.A. Sigman, X. Wang, Y. Lu, *J. Am. Chem. Soc.* 123 (2001) 6945–6946.
- [58] S. Tripathi, M.J. O'Neill, A. Wilks, T.L. Poulos, *J. Inorg. Biochem.* 128 (2013) 131–136.
- [59] M.J. Lee, D. Schep, B. McLaughlin, M. Kaufmann, Z. Jia, *J. Mol. Biol.* 426 (2014) 1936–1946.
- [60] M.J. O'Neill, A. Wilks, *ACS Chem. Biol.* 8 (2013) 1794–1802.
- [61] A.P. Kaur, I.B. Lansky, A. Wilks, *J. Biol. Chem.* 284 (2009) 56–66.
- [62] D.R. Block, G.S. Lukat-Rodgers, K.R. Rodgers, A. Wilks, M.N. Bhakta, I.B. Lansky, *Biochemistry* 46 (2007) 14391–14402.
- [63] M.N. Bhakta, A. Wilks, *Biochemistry* 45 (2006) 11642–11649.
- [64] K.D. Barker, K. Barkovits, A. Wilks, *J. Biol. Chem.* 287 (2012) 18342–18350.
- [65] A. Wilks, *Arch. Biochem. Biophys.* 387 (2001) 137–142.
- [66] E.E. Wyckoff, G.F. Lopreato, K.A. Tipton, S.M. Payne, *J. Bacteriol.* 187 (2005) 5658–5664.
- [67] A.P. Kaur, A. Wilks, *Biochemistry* 46 (2007) 2994–3000.
- [68] H. Ashkenazy, E. Erez, E. Martz, T. Pupko, N. Ben-Tal, *Nucleic Acids Res.* 38 (2010) W529–W533.